In-vitro and *in-vivo* establishment and characterization of bioluminescent orthotopic resistant human osteosarcoma models in NSG mice and resistance mechanisms

Authors

Maria Eugenia Marques da Costa[1,2,3,4], Antonin Marchais[1,2,3], Anne Gomez-Brouchet[5,6], Estelle Daudigeos-Dubus[1,2,3], Bastien Job[6], Noémie Assoun[1,2,3], Olivia Fromigué[1,3,7], Conceição Santos[8], Birgit Geoerger[1,2,3], Nathalie Gaspar[1,2,3]

[1] Gustave Roussy, Université Paris-Saclay, 94805 Villejuif, France

[2] CNRS UMR8203, 94805 Villejuif, France

[3] Université Paris Sud, 91400 Orsay, France

[4] CESAM & Department of Biology, University of Aveiro, 3810 Aveiro, Portugal

[5] IUCT-Oncopole, CHU and University of Toulouse, Pathology department, 31100 Toulouse, France

[5] CNRS UMR5089, 31077 Toulouse, France

[6] INSERM, US23, Gustave Roussy, 94805 Villejuif, France

[7] INSERM, UMR981, Villejuif, 94805, France

[8] Department of Biology, Faculty of Sciences, University of Porto, 4000 Porto, Portugal

Running title: Bioluminescent orthotopic resistant osteosarcoma CDX models

Key words: bone tumor, cell-derived xenograft, bioluminescence, resistance, methotrexate, doxorubicin, MDR1, DHFR

Financial support : Etoile de Martin association, la Ligue contre le cancer, Société Française de lutte contre les Cancers et les leucémies de l'Enfant et l'adolescent (SFCE), Fédération Enfants et Santé and Une Main Vers l'Espoir association. The Portuguese Foundation for Science and Technology (FCT, www.fct.pt) through the PhD fellowship to Maria Eugénia Marques da Costa (SFRH/BD/89137/2012).

Corresponding authors

Nathalie GASPAR, MD, PhD

Vectorology and Anticancer Therapies, CNRS UMR 8203, Paris-Sud University, Gustave Roussy, Paris-Saclay University, 94 805 Villejuif, France

Department of Oncology for Children and Adolescents, Gustave Roussy, 94805 Villejuif, France

114 rue Edouard Vaillant, 94805 Villejuif cedex, France

Phone + 33 1 41 11 41 66

E-mail: nathalie.gaspar@gustaveroussy.fr

Conflict of Interests

The authors declare no potential conflicts of interest.

The financial supporters had no role in study design, data collection and analysis, decision to publish, or preparation of the manuscript.

Category: Research Articles

Abstract - 231/250 words

Text - 4796/5000 words

Tables and figures - 7/7

References - 36/50

Supplementary data - 7/7

Abstract

Osteosarcoma is the most common bone malignancy with a peak incidence at adolescence. Despite current treatment strategies including chemotherapy and surgery, long-term survival has reached a plateau; chemo resistance and metastatic spread remain the major challenges. Our aim was to develop and characterize *in-vitro* resistant models to common osteosarcoma chemotherapy, decipher the mechanisms of resistance and establish *in-vivo* bioluminescent orthotopic cell-derived xenografts (CDX) to compare their *in-vivo* behavior to their parental counterparts.

Continuous increasing drug concentration cultures resulted in five methotrexate- and one doxorubicin-resistant *in-vitro* models. Different mechanisms of acquired resistance to methotrexate according to the genetic background of the cell lines were identified (decreased SCL19A1, increased DHFR). PgP up-regulation was the main mechanism detected in HOS-R/DOXO. Differential analysis of gene expression (RNAseq) and copy number abnormalities (aCGH) revealed modulation of different pathways implicated in metastatic potential (e.g. Fas and several MMPs). Resistant bioluminescent orthotopic CDX models (HOS-R/MTX, HOS-R/DOXO and Saos-2-B-R/MTX) were injected intratibially into NSG mice. At primary tumor site, both HOS and Saos-2-B resistant models behaved in the same way as their parental counterpart, although HOS showed initial difficulties to adapt *in-vivo*. All resistant-CDX models exhibited a slower growth rate and lower metastatic spread than the parental-CDX, and retained resistance without drug pressure, as seen in *in-vitro* culture.

These models represent valuable tools to explore resistance mechanisms and develop new therapies in osteosarcoma, in order to improve patient survival.

Introduction

Osteosarcoma is the first primary malignant bone tumor that predominantly occurs during adolescence(1,2). Standard treatment combines neoadjuvant and post-operative chemotherapy with complete surgery of all primary and metastatic sites. No improvement has been seen in prognosis for almost five decades. Treatment failure is usually due to metastatic relapse. The presence of metastases at diagnosis and poor histological response to neoadjuvant chemotherapy are risk factors of relapse(1,3–5). Resistance to therapy, both intrinsic (phenomenon present prior to chemotherapy administration) and acquired (revealed after chemotherapy administration), contributes to treatment failure and recurrence. Several mechanisms of chemoresistance have been reported in osteosarcoma from drug specific mechanisms to broader mechanisms(6). However, the link between resistance to chemotherapy and metastatic phenotype remains unclear.

The aim of the study was to establish and characterize resistant osteosarcoma models to common chemotherapeutic agents, and analyze their behavior comparatively to their parental counterparts *in-vitro* and *in-vivo* in a bone orthotopic setting.

Methods

Cells culture

Five human osteosarcoma cell lines with different genetic background were used: HOS (TP53 mutated, wild-type RB1, CDKN2A homozygous loss), 143B (HOS virally transfected with Ki-ras oncogene), Saos-2 (TP53 deleted, RB1 mutated, wild-type CDKN2A), MG-63 (TP53 first intron rearrangements, wild-type RB1, CDKN2A homozygous loss) and IOR/OS18 (TP53 deletion>EX3/EX4, CDKN2A homozygous loss, wild-type RB1)(7,8). The 143B line was purchased from the American Type Culture Collection (ATCC, Virginia, USA), HOS, Saos-2, IOR/OS18 and MG-63 lines were kindly provided by the European consortium Innovative Therapeutics for Children with Cancer (ITCC). Saos-2 cells issued from two different culture batches, exhibiting slightly different CGH profiles (supplementary-Fig.S1). We carried on the experiments with both, and named the second one Saos-2-B.

Cells were cultured in Dulbecco's modified Eagle medium (DMEM, Invitrogen, Saint Aubin, France) supplemented with 10% (v/v) fetal bovine serum (FBS, Invitrogen) at 37˚C in a humidified atmosphere (5%CO_2 and 95%air), in mycoplasma free conditions.

Compounds

Doxorubicin (DOXO), methotrexate (MTX), cisplatin (CISP), etoposide (ETOP), vincristine (VCR) and verapamil (VER) were purchased from Sigma Aldrich (Lyon, France), mafosfamide (MAF) from Toronto Research Chemicals Inc (TRC) (Toronto, Canada) and cabozantinib (Cabo) from LC Laboratories (Woburn, Canada). All compounds were solubilized in dimethyl sulfoxide (DMSO; Sigma Aldrich), except cisplatin, solubillized in N,N-dimethylformamide (DMF; Sigma Aldrich), at 10mM stock solution, and stored at -20ºC.

***In-vitro* development of chemotherapy resistant osteosarcoma cell lines.**

Cells were seeded into 6-well plate at 100,000 cells/well (HOS, 143B, MG-63) or 120,000 cells/well (IOR/OS18, Saos-2 and Saos-2-B) in DMEM supplemented with 10% FBS, then exposed continuously to an initial concentration of 0.01µM DOXO or

0.07µM MTX. In parallel DMSO treated cells (parental) were seeded at the same conditions and used as controls. The medium was changed twice a week, and passages (1:10) were performed when cells reached 80% confluence. The MTX concentration was progressively increased up to 0.3µM for MG-63 and 1µM for all other lines; DOXO concentration up to 1.3µM for HOS. The resistant lines were maintained in culture with the maximal tolerated drug concentration and named as “Drug-ON” cell lines. Drug pressure was stopped after resistance confirmation, and resistant cells were cultured in drug free medium for minimum nine weeks, designed as “Drug-OFF” cell lines. The same experiments were performed with MAF. Cells were treated for minimum 2 months to an initial concentration of 2.5µM without success.

In-vitro cell proliferation and cell viability assays

Parental and resistant derived HOS, 143B, MG-63 and IOR/OS18 lines were seeded at 5,000 cells/well, and cells derived from Saos-2 and Saos-2-B at 10,000 cells/well in a 96-well plate in DMEM supplemented with 10% FBS for both assays.

Cell proliferation rate and doubling time were assessed using the IncuCyte live-cell imaging system (Essens Bioscience, Birmingham, UK). Phase-contrast photographs were collected for 72h.

The day after seeding, cells were incubated in the presence of a range of drug concentrations for 72h (from 0 to 100µmol/l for DOXO, ETOP, MAF and Cabo; 0 to 50µmol/l for CISP; 0 to 500µmol/l for MTX; and 0 to 10µmol/l for VCR). Verapamil was used at 5µmol/l and cabozantinib at 0.1µmol/l, to revert PgP function. Cell viability was evaluated using the CellTiter 96 Aqueous One Solution Cell Proliferation Assay (MTS assay) (Promega, Charbonnieres, France), according to the manufacturer instructions. The half-maximal inhibitory concentration IC_{50} was determined using the GraphPad Prism5 software (Graphpad Software Inc, La Jolia, CA, USA). The resistance index (RI) was defined as the ratio of IC_{50} of resistant cell line/IC_{50} of parental cell line.

Wound-healing assay

Cells were seeded at 10,000 cells/well (HOS, 143B, MG-63 and IOR/OS18), or at 20,000 cells/well (Saos-2 and Saos-2-B) in 96-well ImageLock tissue culture plates (Essen BioScience) in DMEM supplemented with 10% FBS. The day after, cell layers

were scratched with the WoundMaker™, washed and then incubated in the presence or not (DMSO control) of the indicated drugs concentrations (0.01µM for MTX, DOXO, CISP and ETOP, or 0.2µM for MAF, IC50 and 10xIC50). The wound-healing was monitored using IncuCyte™ system for 48h. Data analyses were performed using Graphpad Prism5 Software (Graphpad Software Inc).

Transfection and cell transduction with luc/mkate2 (transgene) *in-vitro*

The procedures were performed in sterile and safety conditions as previously described (9). Briefly, parental and resistant HOS and Saos-2-B cell lines were stably transduced with Luc/mKate2.

Orthotopic bioluminescent CDX models

Animal experiments were approved by the CEEA26, CEEA PdL N°6 Ethics Committee and the French Ministry of Agriculture (APAFIS#1648-2015090713516480) and performed under the conditions established by the European Community (Directive 2010/63/UE).

The parental cell lines (HOS-Luc/mKate2 and Saos-2-B-Luc/mKate2) and their resistant counterparts to either MTX (HOS-Luc/mKate2/MTX and Saos-2-B-Luc/mKate2/MTX) or DOXO (HOS-Luc/mKate2/DOXO) were established into 7 week-old immuno deficient NSG mice by unilateral intratibial injection ($1.5x10^6$ cells in a matrigel solution at 4mg/ml), as previously described(9,10). Buprenorphine at 0.3mg/kg was applied in addition to the general anesthesia (3% isoflurane).

Mice were monitored clinically every week, for general symptoms. At the sacrifice day, xenografts were collected and processed for histological analyses or immediately snap-frozen in liquid nitrogen and stored at -80°C for subsequent RNA extraction. Some primary tumor of resistant-CDX were collected, mechanically dissociated, and cultured *in-vitro* in DMEM supplemented with 10% FBS.

***In-vivo* and *ex-vivo* imaging (computed tomography-CTscan and bioluminescence-BLI)**

In-vivo and *ex-vivo* images were acquired using IVIS SpectrumCT (Perkin Elmer, Courtaboeuf, France) as previously described(9). Briefly, NSG mice under anesthesia (3% isoflurane) were injected intraperitoneally with 150mg/kg D-luciferin

(Beetle luciferin, Promega). Whole mice bodies were imaged for primary tumor and metastases detection (BLI and CTscan). After sacrifice, legs, lungs, and spleen were immersed in 150µg/ml D-luciferin and imaged individually. Organs were then washed in PBS and fixed in a 4% paraformaldehyde before paraffin embedding.

Histological analysis and immunohistochemistry (IHC)

Formaldehyde-fixed-paraffin-embedded (FFPE) tissue sections (4µm) were either stained with hematoxylin-eosin-safranin (HES) for morphology, or processed for immunohistochemistry. Briefly, FFPE tissue sections were deparafinized and rehydrated using a series of xylene and ethanol washes. After heat-induced antigen retrieval (citrate buffer pH7.3), tissue sections were incubated with primary specific antibody. The signal was revealed using the peroxidase/diaminobenzidine Klear mouse kit (Diagomics, Blagnac, France), according to the manufacturer's recommendations. Primary antibodies were: mouse anti-firefly luciferase monoclonal antibody (1:200, ThermoFisher Scientific, MA, USA) and mouse monoclonal anti-human MDR1 antibody (1:20, Merck Millipore, Fontenay-sous-Bois, France). Single representative whole tumor tissue section was digitized using a slide scanner NanoZoomer 2.0-HT (Hamamatsu Photonics, Massy, France). Histology was reviewed by a bone expert pathologist. Normal human kidney and IGR-N91-Luc-neuroblastoma cells(11) were used as positive controls for MDR1 and luciferase staining, respectively.

Nucleic acid extraction

Cells were washed in PBS, collected with 450µl of RLT solution (Qiagen, Hilden, Germany)+β-mercaptoethanol (10%) and stored at -80°C. DNA and RNA from cells and from CDX samples were isolated using AllPrep DNA/RNA mini kit (Qiagen) according to manufacturer's instructions. Quantification and qualification were performed using Nanodrop 2000 spectrophotometer (Thermo Fisher Scientific, MA, USA) and Bioanalyzer DNA 7500 (Agilent, CA, USA).

Oligonucleotide comparative genetic hybridization array (aCGH) assay

Sex-matched normal DNA from a pooled human female or male (Promega) was used as a reference. Oligonucleotide aCGH processing was performed according to

manufacturer's protocol (version 7.5; http://www.agilent.com). Equal amounts (500ng) of tumor and normal DNAs were fragmented with AluI and RsaI (Euromedex, Souffelweyersheim, France) and labeled with cyanine Cy3-deoxyuridine triphosphate (dUTP) or Cy5-dUTP. Hybridization was carried out on SurePrint G3 Human CGH Microarray 4x180K (Agilent Technologies, CA, USA) arrays for 24h at 65°C in a rotating oven (Robbins Scientific, CA, USA) at 20rpm and followed by appropriate washing steps. Glass microarrays was scanned with an Agilent G2505C DNA Microarray scanner at 100% PMT with 3µm resolution at 20°C in low ozone concentration environment. Data were extracted from scanned TIFF images using the Feature Extraction software (v11.5.1.1, Agilent), along with protocol CGH_1105_Oct12. All further data manipulations were performed under the R statistical environment in v3.4 (http://cran.r-project.org).

Raw intensities were normalized according to their dye composition (Cy3 fitted over Cy5). Data were transformed to log2(Test/Ref) and normalized according to their local GC content through a lowess regression. Resulting profiles were segmented with the CBS algorithm(12) implemented in the DNAcopy package (v1.42) using default parameters. Profiles were centered using the most centered out of the three most populated peaks of the smoothed log2(Test/Ref) distribution density. Aberration levels were called by setting a log2(Test/Ref) threshold automatically adapted to the internal noise for each profile, considered as one-fourth of the median value of the absolute differences between consecutive log2(Test/Ref) measures along the genome. Segmented, called profiles were then aggregated and hierarchically clustered using the Pearson distance and Ward aggregation method. Profile comparisons were performed, for each pair, first by performing a linear regression of the profile with the lowest dynamics (measured as its interquartile range) to the profile with the highest one; the probe-to-probe direct difference of the log2(Test/Ref) of the two profiles was then computed, and the differential profile was segmented and called as described previously. Genomic regions called as different in the pair of profiles were annotated using the UCSC annotation tables (cytoBandIdeo, cpgIslandExt, wgRna, refGene, dgvMerged), corresponding to the hg19 genome build.

RNA sequencing (RNAseq)

RNAseq analysis was performed as previously described(13). RNAseq libraries were prepared with TruSeq Stranded mRNA kit following recommendations: the key steps consisted of PolyA mRNA capture with oligo dT beads 1µg total RNA, fragmentation to approximately 400pb, DNA double strand synthesis, and ligation of Illumina adaptors amplification of the library by PCR for sequencing. Libraries sequencing were performed using Illumina sequencers (NextSeq 500 or Hiseq 2000/2500/4000) in 75bp paired-end mode. Quality of stranded pair-ended RNAseq libraries was evaluated with fastqc (https://www.bioinformatics.babraham.ac.uk/projects/fastqc/). Reads were mapped with Salmon v0.8.1(14) using GRCh37 ENSEMBl mRNA dataset as reference sequences. Differential mRNA expression was measured with DESeq2 R package from raw read count table(15).

Differential mRNA expression lists were compared using Venny diagram produced by Venny 2.1.0 (http://bioinfogp.cnb.csic.es/tools/venny/). Toppfun website was used for functional enrichment analysis (https://toppgene.cchmc.org/enrichment.jsp).

Reverse Transcription-quantitative PCR (RT-qPCR)

Total RNA (1µg) were reversely transcribed into cDNA using M-MLV Reverse Transcriptase (ThermoFisher Scientific), according to the manufacturer's recommendations. *A*mplifications monitored with StepOnePlus PCR System (Applied Biosystems, Villebon-sur-Yvette, France), were performed using Maxima SYBR Green/ROX qPCR kit (ThermoFisher Scientific), and with a first step at 95°C for 10min followed by 40 cycles with 95°C for 15sec and 60°C for 1min. Melting curve was performed at the end of the PCR (95°C for 15sec, 60°C for 1min and 95°C for 15sec) to identify unique PCR products. The sequences of the specific primers are described in supplementary-Table.SI. Glyceraldehyde-3-phosphate dehydrogenase (GAPDH) from Invitrogen was used as standard. Data were analyzed by the relative quantification method using the $2^{-\Delta\Delta Ct}$ formula(16).

Western-Blot

Parental and resistant Drug-ON and Drug-OFF cell lines were seeded into 100*20mm culture dish at 130,000 cell/dish in DMEM supplemented with 10% FBS. Cells were collected when they reached 80-90% of confluence by trypsinization, followed by PBS wash, re-suspended in 100µl of lysis buffer (10ml of TNEN 5mM buffer add ½ protease inhibitor pill, 50µl of NaF and 50µl of Orthovanadate) and

stored at -20ºC. Protein was extracted and measured with Pierce BCA Protein Assay Kit (ThermoFisher Scientific).

Western-blot analysis was performed using specific primary antibody against topoisomerase-II alpha/beta (TOPO2) (1:1000, anti-topoisomerase-II alpha + topoisomerase-II beta Antibody, abcam, Paris, France), anti-dihydrofolate reductase (DHFR) (1:1000, abcam) and β-Actin (13E5) Rabbit mAb (1:1000, Cell Signaling Technology, Schuttersveld, Netherlands). Appropriate secondary antibodies (Cell signaling) at 1:5000 dilution were used, followed by visualization with the enhanced chemiluminescence ECL reagent (ThermoFisher Scientific) and imaged with ChemiDoc™MP image system (Bio-Rad, CA, USA). Signal intensities were quantified with the Image Lab version5 (Bio-Rad).

Statistical analysis

Data were shown as the mean±standard error of mean (SEM) of three independent experiments performed using Graphpad Prism®5 Software (Graphpad Software Inc). The one-way ANOVA analysis was used to compare the groups. $P<0.05$ was considered to indicate a statistically significant difference.

Results

Development of *in-vitro* osteosarcoma cell lines resistant to chemotherapy

In order to establish resistant cell lines, a panel of six osteosarcoma cell lines were exposed to increasing concentrations of MTX or DOXO. Parental and resistant lines were assessed for their response to chemotherapy in terms of cell viability, migration ability, and resistance index. IC50 of parental and resistant lines are given in supplementary-Table.SII. Acquired resistance to MTX developed in 5/6 lines (83%) within 3 months and reached up to 14xIC50 (1µM) for HOS, Saos-2, Saos-2-B, 25xIC50 (1µM) for 143B or 5xIC50 (0.03µM) for MG-63, after 9 months of exposure (Fig1A). The IOR/OS18 cell line exhibited an intrinsic high level of resistance to MTX (IC50=1µM). No further resistance to MTX was obtained. Acquired resistance to DOXO was achieved in only 1/6 cell lines (17%) and after a 4 months exposure time. HOS-R/DOXO was resistant up to 5xIC50 (1.3µM) (Fig1B). Under continuous exposure to increasing concentrations of MAF, above the IC_{50}, up to 2 months none of the six cell lines were able to survive.

We then evaluated the stability of this acquired chemotherapy resistance by culturing resistant lines in medium without the compound for at least 9 weeks. Under continuous drug pressure (Drug-ON) all lines had high RI to MTX > 37, while Drug-OFF cell lines exhibited variable behavior (Fig.1A). HOS-R/MTX, 143B-R/MTX and Saos-2-R/MTX maintained RI at a similar level (from 150 to 143, 103 to 116 and from 41 to 35, respectively), RI of Saos-2-B-R/MTX and HOS-R/DOXO decreased (from 38 to 24 and from 224 to 87, respectively), whereas MG63-R/MTX RI normalized in two weeks (from 71 to 3) (Fig.1A).

No differences in morphology, growth rate or migration ability were detected between the MTX-resistant cell lines and their parental counterparts (supplementary-Fig.S2). HOS-R/DOXO grew and migrate more slowly than its parental line (doubling time=45h *vs.* 25h; 40h migration=around 70% vs 20% respectively) (supplementary-Fig.S2).

Cross-resistance to other drugs

The acquisition of a cross-resistance to other compounds was evaluated in resistant cell lines in Drug-ON and Drug-OFF culture conditions (Fig.1A/B). Cells were exposed to different concentrations of ETOP, CISP, DOXO, MTX, MAF, VCR or to the multi-tyrosine kinase inhibitor cabozantinib (Cabo) for 72h before cell viability evaluation.

Cross-resistance was not detected with any tested compound in the MTX-resistance lines Drug-ON (Fig.1A). Similar RI were observed in Drug-ON and Drug-OFF cells, except for MG-63-R/MTX. Surprisingly, in Drug-OFF culture conditions, the MG-63-R/MTX exhibited a 5- to 10-fold increased RI for MAF, CISP and ETOP (Fig.1A).

For HOS-R/DOXO, cross-resistance was detected with ETOP (RI=276), VCR (RI=172) and MTX (RI=12) (Fig.1B). The co-treatment with the verapamil a PgP inhibitor, allowed to almost abolished the resistance to DOXO and VCR (Fig.1C), but not to ETOP or MTX (data not shown), suggesting the involvement of a PgP (MDR1/ABCB1) multi-drug resistance phenomenon. The weaker PgP inhibitor, cabozantinib did not modify the RI of any drug tested (data not shown). A strong increase in MDR1 mRNA levels was detected by RT-qPCR in the resistant HOS-R/DOXO cells compared to the parental line (Fig.1D). A decrease in toposisomerase-II (TOPO2A) protein level was detected by western-blot in the R/DOXO Drug-ON and Drug-OFF cells compared to the parental line (Fig.1E).

Copy number and gene expression differential analysis between resistant and parental lines

Based on copy number abnormalities (CNA-aCGH) and gene expression profiles (GE-RNAseq), the resistant lines clustered according to their genetic background rather than the resistance mechanisms (clustering analysis) (supplementary-Fig.S1)

Common acquired CNA were seen in MTX-resistant lines issued from similar genetic background (HOS/143B, Saos-2/Saos-2-B and MG-63, respectively), involving different genes known to be implicated in MTX resistance, according to each line. HOS-R/MTX and 143B-R/MTX lines gained chromosomes 5q region containing DeHydroFolate Reductase (DHFR) (Chr5:80,626,228-80,654,983); lost chromosome 21q region containing Reduced Folate Carrier gene (SLC19A1/RFC) (chr21: 46,934,628-46,962,385) and COL18A1 (Chr21: 45,405,137-45,513,720) and lost 2q containing UGT1A (Chr2: 233,585,439-233,773,299) (supplementary-Fig.S3). 143B-R/MTX line presented a break point in SCL19A1 gene, and both HOS-R/MTX and 143B-R/MTX in the close COL18A1. MG-63-R/MTX exhibited an amplification of DHFR-containing region, without CNA modification of SLC19A1/RFC, MTHFR and UGT1A-containing regions. Resistant Saos-2-R/MTX and Saos-2-B-R/MTX gained the MTFRH-containing region (chr1:564,423-17,221,943) without DHFR, SLC19A1/RFC and UGT1A locus modifications. Differential GE analysis (Fig.2A) between MTX-resistant lines versus their parental counterpart showed no change in MTHFR mRNA expression, while increased DHFR and decreased SLC19A1/RFC mRNA expressions were seen in all MTX-resistant lines (although the SLC19A1/RFC mRNA level remained high in MG63-R/MTX), irrespective of MTX pressure (Drug-ON and OFF) (Fig.2B) and of observed CNA changes. No SLC19A1/RFC inactivating mutation was detected (RNAseq analysis). DHFR protein levels (WB) increased in all MTX-resistant lines Drug-ON compared to parental counterpart (Fig.2B), then decreased in Drug-OFF condition to the parental levels, except for HOS-R/MTX and 143B-R/MTX that had a gained DHFR region. Differential GE analysis (Fig.3A/B) between all MTX-resistant line Drug-OFF versus their parental counterpart, also highlighted pathways implicated in osteosarcoma oncogenesis (RTN1)(17), in more general mechanisms of chemotherapy resistance such as up regulations of several genes implicated in transcription (ESF1, CCND1, NFE2L3, ETV1, NFIL3), in the MAPK pathway (EFNA1, TPD52L1, EDIL3), or SSBP2 (Chr5:81,413,021-

81,751,797) which participate in DNA damage response and maintenance of genome stability and has a role in the telomeres protection(18), but also in pathways which suggest less metastatic potential (up regulation of Fas(19) and down regulation of MMP3) and promote apoptosis (up regulation of Fas, down regulation of EIF3B)(20,21).

The acquired CNA in the unique doxorubicin resistant line HOS-R/DOXO translated in mRNA GE expression with up-regulation of gene involved in acquired gained chromosomal regions (Fig.3). The most significantly gained regions in HOS-R/DOXO compared to parental line were on chromosomes 7:86,259,619-88,276,590 (Diff.l2r +4.7369) containing ABCB1/MDR1 and ABCB4, and on chromosomes 11:102,449,766-103,152,951 (Diff.l2r +3.1626) containing several matrix metalloproteinases (MMPs) (Fig.3C). In GE, ABCB1/MDR1 had the highest significant positive fold change (log2 Fold Change +6.49; adjusted p value 6.63E-100) followed by MMP13 (log2 Fold Change +6.40; adjusted p value 5.35E-88). Several other regions with acquired CNA contained multiple multidrug resistance genes also up regulated in the resistant line in GE. The alpha/beta hydrolase MEST has the highest significant negative fold change (log2 Fold Change -9.94; adjusted p value 8.78E-173) and has been implicated in osteosarcoma oncogenesis(22,23). Decreased mRNA expression of RFC and increased mRNA expression of DHFR, although not significant, might participate to the slight MTX resistance observed in the DOXO-resistant line.

Cancer stem cell markers (SOX2, OCT4, SSEA4, NANOG and ABCG2)(24) were not modified in MTX-resistant lines while SOX2 was up-regulated in HOS-R/DOXO compared to its parental line (log2FoldChange 1.89, adjusted p value 6,45E-04).

In-vivo primary tumor characteristics of HOS and Saos-2-B bioluminescent orthotopic parental and resistant-CDX models

Parental and resistant HOS and Saos-2-B lines stably transduced with Luc/mKate2 vector to express luciferase (above 90% Luc/mKate2 positive cells) (Supplementary-Fig.S4) were injected into NSG mice at an orthotopic site (intratibial). Primary tumor growth and metastatic dissemination were followed using IVIS SpectrumCT system (bioluminescence and CTscan).

Bone engraftment rates of HOS-R/MTX and parental counterpart were similar (100%), whereas the HOS-R/DOXO-CDX had a slightly lower engraftment rate (66%)

(Table.I). The HOS-resistant lines had more difficulties to adapt to the *in-vivo* bone environment, with an initial decrease in *in-vivo* bioluminescence (up to 27 days), followed by a slightly faster growth compared to the HOS-parental-CDX (Fig.4A). However, in general both parental and resistant models exhibited similar primary tumor growth (Fig.4A). Bone engraftment rate of Saos-2-B-R/MTX and parental-CDX were comparable (83% *vs.* 100% respectively) (Table.I).

The resistant models retained the primary tumor-induced bone abnormalities of their parental counterpart in CTscan (Fig.4B). The slow growing osteolytic HOS-CDX were confined to bone, while the fast growing Saos-2-B-CDX induced aggressive osseous and extraosseous mass with osteocondensation deforming the leg. HES staining confirmed the osteoblastic phenotype of all models with however, some fibroblastic component (Fig.4B) and no morphological differences between parental and resistant-CDX. *In-vivo* and *ex-vivo* bioluminescence, CTscan and histology (HES and luciferase staining), confirmed that the changes observed were caused by human osteosarcoma cells (Fig.4B; supplementary-Table.SIII). The different models revealed tumor-bearing tibia bone structure abnormalities similar to those observed in the human osteosarcoma patients. PgP protein expression, was detected by IHC in HOS-R/DOXO-CDX but not in the HOS-parental-CDX (Fig.4C) or HOS-R/MTX-CDX (data not shown) primary tumors.

In-vivo **metastatic behavior of the resistant orthotopic bioluminescent-CDX models**

Metastatic foci were detected by *in-vivo* bioluminescence in all CDX models as early as 30 days after intratibial injection (Fig.5A) except for HOS-R/MTX-CDX where metastases were detectable only by *ex-vivo* bioluminescence (Fig.5B-top-panel). Metastases in parental-CDX models grew faster than in resistant-CDX models, without correlation with the primary tumor growth rate and size (Fig.5A). At sacrifice (day 84 and 127 for parental and Saos-2-B-R/MTX-CDX, respectively, and day 160 for all HOS models), combined *ex-vivo* bioluminescence and histology confirmed lung metastases in all models (Fig.5B). Lung metastases were bigger and more frequent in Saos-2-B-parental-CDX than in HOS-parental-CDX, and in parental-CDX compared to their resistant-CDX counterparts. Unique bone metastases on the opposite leg (not injected) and unusual spleen metastases were detected in all models except in HOS-R/MTX-CDX. HES did not detect morphological differences

between parental and resistant-CDX (Fig.5B). Metastases were not detected by CTscan due to its resolution, however HES staining confirmed the osteosarcoma nature of metastases detected by bioluminescence (Fig.5B; supplementary-Table.SIII).

In-vitro behavior of secondary cultures issued from CDX models

After sacrifice, cells isolated from primary tumors of each CDX model were cultured for two *in-vitro* passages. All resistant-CDX-derived cells grew *in-vitro*. Drug response was assessed and RI of *in-vitro* originally resistant cells and resistant-CDX-derived cells were variable. RI either decreased (HOS-R/DOXO-CDX-cells RI=224 and 42, respectively), increased (HOS-R/MTX-CDX-cells; RI=150 and >2500), or was stable (Saos-2-B-R/MTX-CDX-cells; RI=38 and 34) (Table.II).

Discussion

Resistance to chemotherapy and metastatic phenotypes are the two main problems in osteosarcoma patients, leading to recurrence and death. We developed *in-vitro* osteosarcoma models, resistant either to MTX (HOS, 143B, MG-63, 2 closed Saos-2/Saos-2-B lines) or DOXO (HOS), by continuous *in-vitro* exposure to these chemotherapeutic agents, adding new models to those described in the literature(2,25–28). We characterized these models and further established *in-vivo* orthotopic CDX models derived from three of these resistant lines and compared their *in-vivo* behavior (primary tumor growth and metastatic potential) to their parental counterparts.

Acquired *in-vitro* resistance establishment was influenced by the nature of the drug, initial cell sensitivity to the drugs but other potential factors(29). High levels of *in-vitro* acquired resistance were frequently obtained with MTX (5/6 cell lines), hardly any with DOXO (1/6 cell lines) and no resistance with MAF. The IOR/OS18 line appeared primarily resistant to all tested drugs, and no further resistance was obtained. Previously published primary culture of low-passage tumor cell derived from patient samples either prior to or after chemotherapy exposure were shown sensitive to DOXO and CISP while resistant to MTX(24).

The incidence and mechanism of acquired resistance may affect cell sensitivity to other drugs, depending on the target, the mechanism of action, or the drug metabolism(30). HOS-R/DOXO line exhibited a multi-drug resistant phenotype, with cross-resistance to other anti-osteosarcoma agents substrate of PgP (e.g. ETOP, VCR), but also to MTX. A reduced MTX sensitivity was previously reported in osteosarcoma doxorubicin-resistant models(25) and associated with down-regulation of RFC expression levels. Cross-resistance is a critical issue at clinical level and different drug combinations might be used to overcome these chemoresistance. Cabozantinib a multi-tyrosine kinase inhibitor used in relapsed osteosarcoma and inhibiting PgP activity in hepatoblastoma cells(31), did not revert the resistance to DOXO in HOS-R/DOXO. The impact on the clinical efficacy of ABCB1/MDR1 and ABCC1 inhibitors which revert *in-vitro* resistance in other doxorubicin-resistant osteosarcoma lines(30), will have to be followed on a multidrug anti-osteosarcoma regimen context in patients (including MTX, DOXO, CISP, ETOP, IFO)(5,32). Cross-resistances with doxorubicin, ifosfamide, epirubicine, theprubicin or paclitaxel has been reported in low and intermediate MTX-resistant Saos-2 lines (RI of 5 and 13, respectively) with low RFC expression(33). In our highly MTX-resistant lines (RI>37), no cross-resistance was detected with the other drugs tested *in-vitro*. Very high RI may select cells with specific mechanisms of resistance to alterations of hydrofolate reductase activity and less permissive counterbalanced mechanisms.

The acquired *in-vitro* resistance phenotypes were associated with modifications at both CNA and GE, in a drug and cell line dependent manner(29), involving genes known to be responsible for resistance to the tested drugs. As expected, ABCB1/MDR1 gain was detectable in HOS-R/DOXO, resulting in upregulation of multi-drug resistant protein PgP. DOXO-resistant cells gained several chromosomic regions associated with mRNA expression up-regulation of the corresponding genes. Such CNA gain were confirmed for chromosome 7 region containing ABCB1/MDR1 and ABCB4, but also several other regions encoding various multiple multi-drug resistance genes, or genes implicated in the apoptotic response to doxorubicin. In the same way, the RNAseq/aCGH analyses revealed that mechanisms of acquired MTX-resistance correlated with CNA, mRNA expression or post-transcriptional regulation of genes linked to the MTX metabolism at different levels. All MTX-resistant cell lines exhibited a down-regulation of mRNA levels of the ubiquitous transporter for folates SCL19A1/RFC and upregulation of DHFR mRNA and protein

expression. Resistance persisted despite drug removal, although at lower level for HOS-R/MTX, and lost in MG-63-R/MTX after two weeks without drug. This resistant phenotype paralleled the mRNA level of SLC19A1/RFC, irrespective of the CNA variation observed, except for MG-63. DHFR protein increase was dependent on the presence of MTX in culture with involvement of post-transcriptional regulation as mRNA levels were up-regulated in the resistant lines Drug-OFF, irrespective of the gain of DHFR region (present in HOS, 143B and MG-63, but not in Saos-2 or Saos-2-B). The link between RB1 expression and MTX-resistance mechanisms previously reported with increased DHFR expression by gene amplification in RB1-expressing osteosarcoma cell lines and RFC expression decrease without DHFR involvement in RB1deficient (not expressing) lines(25), did not fully apply to our models. All these observations question the impact of concomitant long-term *in-vivo* administration of drug combinations as used in patient first line treatment and the link between resistant phenotype and metastatic potential.

The significance for the patients is unclear and probably more complexity is added by potential additional cellular/molecular programs modified on acquired resistant lines, not directly linked to the mechanism of action and metabolism of one drug. Several, more general cellular and biological pathways were modulated in the chemoresistant lines related to cell adhesion/motility, extracellular matrix organization/degradation/ composition, and cellular microenvironment. These processes, not fully assessed *in-vitro*, might affect the resistant-cell behavior *in-vivo*. In DOXO and MTX-resistant osteosarcoma lines, Fas expression was increased, suggesting a decreased *in-vivo* metastatic potential(19). Similarly, MMP3 decrease in MTX-resistant cell lines suggested less invasive potential, while MMP13 increase in the DOXO-resistant line suggested a more invasive phenotype compared to their respective parental lines. In our *in-vitro* resistant models, no modification of cancer stem cell marker was observed as it has been seen in PDX models(24). In addition, the bone microenvironment is known to have a key role in osteosarcoma progression(34), and has been shown to influence drug sensitivity in osteosarcoma syngeneic models(35) and might influence resistance phenotype(29).

We developed *in-vivo* orthotopic intratibial bioluminescent parental and resistant-CDX models in NSG mice, with the experimental procedure used previously(9). The different primary tumor bone behavior (slow growing osteolytic HOS-CDX, fast

growing osteocondensed Saos-2-B-CDX), metastatic potential (faster metastatic spread in Saos-2-B-CDX than in HOS) and morphology(9) were retained by the respective resistant models. Most importantly all resistant-CDX presented different metastatic behaviors than parental-CDX, with a slower and lower lung metastatic spread. Similar behavior has been observed with other *in-vivo* models of metastatic spread by direct intra-venous injections of doxorubicin-resistant osteosarcoma U2OS and Saos-2 variants (MDR1 overexpression by gene amplification) in athymic nude mice, when resistant-cells were injected straight after treated medium culture but not when cultured in a drug free medium for a week before injection(36). In our CDX-models, secondary cultures of the resistant lines after sacrifice retained their resistant phenotype. Time intervals between cell injection and detection of primary tumor growth and metastatic spread are still compatible with drug testing *in-vivo*.

These resistant-CDX models are useful tools to evaluate the response to new drugs in osteosarcoma and complement the few preexisting osteosarcoma models. This experience is currently translated to the development of Patient-derived xenografts models from relapsed osteosarcoma samples which will bring complementary knowledge on human osteosarcoma drug resistance, while syngeneic (mice or dog) or humanized osteosarcoma models might partially give access to the immunity role in osteosarcoma resistance to treatment.

Author's contributions

Conception and design: MC, NG
Development of methodology: MC, NG
Acquisition of data: MC, AM, BJ, NA, AB-G
Analysis and interpretation of data: MC, NG
Writing of the manuscript: MC, NG
Review and/or revision of the manuscript: All authors
Technical or material support: ED, NA
Study supervision: NG

Acknowledgments

We thank the Platform of Preclinical Evaluation for providing immunocompromised mice and animal care and the platform of Genomic (mainly Noemie Pata-Merci and Betty Leite) at Gustave Roussy, Olivia Bawa for performing the histology slides, Irene Villa for having scanned the histology slides and Alec Guyomard for some genetic samples analysis. To Valerie Roufiac for help on IVIS spectrumCT system function and Brenda Mallon for critical reading of the manuscript

Table and Figures legends

Figure 1: Acquired *in-vitro* resistance to methotrexate and doxorubicin in osteosarcoma cell lines and cross-resistance with other chemotherapeutic agents used in osteosarcoma. Resistance Index (RI) is defined as the ratio IC_{50} of resistant line / IC_{50} of the corresponding parental line. **A-** RI of the methotrexate (MTX) and doxorubicin (DOXO) resistant lines, drug-ON and drug-OFF (for 9 weeks). **B-** Cross-resistance to other drugs used in osteosarcoma for the MTX and DOXO resistant lines drug-ON (doxorubicin, methotrexate, etoposide, cisplatin, mafosfamide, cabozantinib and vincristine). **C-** Resistance reversion by PgP inhibitors in HOS-R/DOXO. PgP inhibitors used: Verapamil (VER) and Cabozantinib (Cabo). **D-** MDR1/ABCB1 (or PgP) mRNA expression in HOS-R/DOXO drug-ON and drug-OFF by RT-qPCR. E- Topoisomerase IIa (TOPO2A) mRNA expression in HOS-parental, HOS-R/DOXO drug-ON and drug-OFF by Western blot. ND- Not done; ETOP- Etoposide; CISP- Cisplatin; MAF- Mafosfamide; VCR- Vincristine. $P<0.05$ was considered statistically significant differences (the values presented in the figures A and B were considered statistically different).

Figure 2: Differential analysis of the MTX-resistant and parental cell lines. A- Heatmap illustrating color-coded expression levels of the most differentially expressed genes from RNA sequencing of MTX-resistant drug-OFF versus parental cell lines. **B-** RFC and DHFR modification in MTX-resistant compared to parental cell lines at Copy Number Abnormalities (CNA; aCGH), mRNA expression (RNA sequencing), and protein level (Western blot – Ratio DHFR/Actin represented by the Y axis and the Ratio Resistant/Parental DHFR expression values showed above corresponding column).

Figure 3: Differential analysis of the DOXO-resistant and parental cell lines. A- Heatmap illustrating color-coded expression levels of the most differentially expressed genes from RNA sequencing of HOS-R/DOXO drug-OFF versus parental cell line. **B-** Genes found significantly enriched for specific chromosomal regions (cytobands). **C-** Direct comparison of HOS-R/DOXO versus HOS-parental CNA profiles. Upper panel: Unscaled CNA profiles for HOS-R/DOXO (blue) and HOS-parental (blue). Middle panel: Same profiles after dynamics scaling of the HOS-parental profile, with significant differences colored in red areas, with corresponding segments positions as blue or red bars. Lower panel: segmentation of the difference profile.

Table I: *In-vivo* primary tumor engraftment and metastatic rate of the resistant (HOS-R/MTX-CDX, Saos-2-B-R/MTX-CDX and HOS-R/DOXO-CDX) and parental (HOS-parental-CDX, Saos-2-B-parental-CDX) orthotopic bioluminescent osteosarcoma cell line derived xenografts.

Figure 4: Primary tumor characteristics of the bioluminescent parental and resistant orthotopic cell-derived osteosarcoma xenograft models developed in NSG mice by intratibial injection. A- Primary tumor *in-vivo* bioluminescence (BLI) detection overtime for parental and resistant-CDX. **B-** Orthotopic osteosarcoma bioluminescent models in NSG mice at time of sacrifice: HOS-CDX (top panel), Saos-2-B-CDX (bottom panel) (both parental-CDX, both R/MTX-CDX and HOS-R/DOXO-CDX). *In-vivo* BLI imaging by IVIS SepectrumCT system of the primary tumor (left leg) compared to the control leg (right leg). *In-vivo* CTscan imaging (CT) by IVIS SepectrumCT system of the normal leg (N) and Primary tumor, showing osteocondensation (plain white arrow) and osteolysis (dotted white arrow), changes were first noted 63, 91 and 77 days after injection for HOS-parental-CDX, HOS-R/MTX-CDX, HOS-R/DOXO-CDX and at day 41 and 49 days after injection for Saos-2-B-parental-CDX and Saos-2-R/MTX-CDX, respectively. Histology (Histo) using Hematoxylin Eosin Safranin (HES) and luciferase staining of the primary tumor and normal bone at 7,45x magnification, showing osteoid matrix (big black arrow) and infiltration by the tumor cells in the bone (small black arrow). **C-** Immunohistochemistry MDR1 protein expression in primary tumor tissue of HOS-parental and HOS-R/DOXO-CDX models. Normal human kidney was used has positive control (image surrounded with black lines).

Figure 5: *In-vivo* metastatic behavior of the bioluminescent parental and resistant orthotopic cell-derived xenografts osteosarcoma models in NSG mice by intratibial injection. A- *In-vivo* metastases bioluminescence (BLI) detection overtime for parental and resistant CDX. **B-** Orthotopic osteosarcoma bioluminescent models in NSG mice at time of sacrifice: HOS-CDX (top panel), Saos-2-B-CDX (bottom panel); Both parental-CDX, both R/MTX-CDX and HOS-R/DOXO-CDX. *In-vivo (*a) and *ex-vivo* BLI of lung (b) and spleen (e) metastases. Lung Hematoxylin Eosin Safranin (HES) (c) and luciferase staining (d) at 1,5x magnification for all HOS-CDX and 0,21 and 10,8x magnification for Saos-2-B-parental-CDX and Saos-2-B-R/MTX-CDX, respectively. Spleen HES (f) and luciferase staining (g) at 10,8 and 0,36x magnification for HOS-parental-CDX and both resistant-CDX, respectively, and 3x for all the Saos-2-B-CDX models. Plain arrows showed metastases

Table.II: Resistance phenotype of the orthotopic resistant osteosarcoma CDX models. Drug sensitivity (IC_{50} and RI) in early secondary cell culture derived from resistant-CDX

models (HOS-R/MTX-CDX-cells, HOS-R/DOXO-CDX-cells and Saos-2-B-R/MTX-CDX-cells) compared to the initial *in-vitro* values. Parental and Resistant drug-ON before introduction in the mice and resistant drug-ON cell line after injection in NSG mice and cultured *in-vitro* after mice sacrifice. * Before or after injection of the cell lines in NSG mice. NA- Not available

Supplementary

Supplementary-Figure.S1: Clustering analysis of the resistant and parental cell lines. A- Hierarchical clustering and heatmap of the copy number abnormalities (CNA) profiles (Pearson distance, Ward construction method). Gains are displayed in blue, losses in red, grey for normality. Amplifications (L2R > 1.5) and deletions (LRR < 1.5) are represented as turquoise and brown dots, respectively. Lower part of the plot represents for the sample population the cumulative frequency of CNA events for gains in blue, and losses in red, along the genome. **B**- First two principal components extracted from principal component analysis (PCA) performed with the gene expression of top 1000 variable genes.

Supplementary-Table.SI: Primers used to amplify topoisomerase IIa (TOPO2A), multidrug resistance protein 1 (MDR1/ABCB1) or P-glycoprotein 1 (PgP) and multidrug resistance associated protein 1 (MRP1/ABCC1) cDNAs by quantitative real-time PCR. Glyceraldehyde 3-phosphate dehydrogenase (GAPDH) was used as control.

Supplementary-Table.SII: Acquired *in-vitro* resistance to methotrexate (MTX) and doxorubicin (DOXO). IC_{50} values of the Parental and resistant (drug-ON and drug-OFF) cell lines to MTX, DOXO and mafosfamide (MAF) as well as to DOXO Resistant (R/DOXO) cell line treated with etoposide (R/DOXO). IC_{50} values were calculated using Prisma version5 using cell proliferation data after 72h of treatment. NA- not applicable, NO- not obtained

Supplementary-Figure.S2: *In vitro* characteristics of HOS and Saos-2-B parental and resistant cell lines to MTX and DOXO. A- Morphology; **B**- Doubling time; **C** -Migration potential with (0.01µM) and without (control) treatment. MTX resistant cell lines were treated with MTX and the cell line DOXO resistant were treated with doxorubicin (DOXO). Parental cell lines were treated with MTX and Doxorubicin. The same procedure was performed for the others cell lines (143-B-R/MTX, Saos-2-R/MTX, MG-63-R/MTX) and with the others compounds (ETOP, CISP, MAF) showing a similar behavior as HOS-R/MTX.

Supplementary-Figure.S3: Direct comparison of HOS-R/MTX, 143B-R/MTX, Saos-2-R/MTX, Saos-2-B-R/MTX and MG-63-R/MTX versus their respective parental CNA profiles. Upper panel: Unscaled CNA profiles for MTX-resistant (blue) versus respective parental (blue). Middle panel: Same profiles after dynamics scaling of each parental profile, with significant differences colored in red areas, with corresponding segments positions as blue or red bars. Lower panel: segmentation of the difference profile.

Supplementary-Figure.S4: Characterization of luciferase-transfected osteosarcoma cells. Data shown for the two osteosarcoma parental cell lines (HOS-parental and Saos-2-B-parental) and for the respectively methotrexate and doxorubicin resistant cell lines (HOS-R/MTX, HOS-R/DOXO and Saos-2-B-R/MTX) after FACS selection showing a rate of more than 90% of luciferase positive cells.

Supplementary-Table.SIII: Morphological and histological characteristics of all osteosarcoma bioluminescent orthotopic CDX: HOS-parental-CDX, HOS-R/MTX-CDX, HOS-R/DOXO-CDX, Saos-2-B-parental-CDX and Saos-2-B-R/MTX-CDX. BLI- *In-vivo* and *ex-vivo* bioluminescence; CT-Computed Tomography; Histo-Histology; FB-fibroblastic subtype; OB- Osteoblastic subtype; HG- High-Grade osteosarcoma; NA- Not Available; ND-Not done; **+** - Positive detection; **-** - Negative detection; Met- Metastases.

References

1. Yang X, Yang P, Shen J, Osaka E, Choy E, Cote G, et al. Prevention of multidrug resistance (MDR) in osteosarcoma by NSC23925. *Br J Cancer* **2014**;110:2896–904.
2. Wang J and Li G. Mechanisms of methotrexate resistance in osteosarcoma cell lines and strategies for overcoming this resistance. *Oncol Lett* **2015**; 9(2): 940–944.
3. PosthumaDeBoer J, van Royen BJ, Helder MN. Mechanisms of therapy resistance in osteosarcoma: a review. *Oncol Discov* **2013**;1-8.
4. Duan Z, Gao Y, Shen J, Choy E, Cote G, Harmon D, et al. miR-15b modulates multidrug resistance in human osteosarcoma *in vitro* and *in vivo*. *Mol Oncol* **2017**; 11(2):151-166.
5. Bielack SS, Smeland S, Whelan JS, Marina N, Jovic G, Hook JM, et al. Methotrexate, Doxorubicin, and Cisplatin (MAP) Plus Maintenance Pegylated Interferon Alfa-2b Versus MAP Alone in Patients With Resectable High-Grade Osteosarcoma and Good Histologic Response to Preoperative MAP: First Results of the EURAMOS-1 Good Response Randomized Controlled Trial. *J Clin Oncol* **2015**; 33(20):2279-87.
6. He H, Ni J, Huang J. Molecular mechanisms of chemoresistance in osteosarcoma (Review). *Oncol Lett* **2014**;7:1352–62.
7. Ottaviano L, Schaefer K-L, Gajewski M, Huckenbeck W, Baldus S, Rogel U, et al. Molecular characterization of commonly used cell lines for bone tumor research: A trans-European EuroBoNet effort. *Genes, Chromosom Cancer* **2010**;49:40–51.
8. Lauvrak SU, Munthe E, Kresse SH, Stratford EW, Namløs HM, Meza-Zepeda LA, et al. Functional characterisation of osteosarcoma cell lines and identification of mRNAs and miRNAs associated with aggressive cancer phenotypes. *Br J Cancer* **2013**;109:2228–36.
9. Marques da Costa ME, Daudigeos-Dubus E, Gomez-Brouchet A, Bawa O, Rouffiac V, Serra M, et al. Establishment and characterization of in vivo orthotopic bioluminescent xenograft models from human osteosarcoma cell lines in Swiss nude and NSG mice. *Cancer Med* **2018**; 7(3):665-676.
10. Uluçkan Ö, Bakiri L, Wagner EF. Characterization of Mouse Model-Derived Osteosarcoma (OS) Cells *In Vitro* and *In Vivo*. *Methods Mol Biol*

2015;1267:297-305.

11. Daudigeos-Dubus E, LE Dret L, Rouffiac V, Bawa O, Leguerney I, Opolon P, et al. Establishment and characterization of new orthotopic and metastatic neuroblastoma models. *In Vivo* **2014**;28:425–34.
12. Olshen AB, Venkatraman ES, Lucito R, Wigler M. Circular binary segmentation for the analysis of array-based DNA copy number data. *Biostatistics* **2004**;5:557–72.
13. Harttrampf AC, Lacroix L, Deloger M, Deschamps F, Puget S, Auger N, et al. Molecular Screening for Cancer Treatment Optimization (MOSCATO-01) in Pediatric Patients: A Single-Institutional Prospective Molecular Stratification Trial. *Clin Cancer Res* **2017**; 23(20):6101-6112.
14. Patro R, Duggal G, Love MI, Irizarry RA, Kingsford C. Salmon provides fast and bias-aware quantification of transcript expression. *Nat Methods* **2017**;14:417–9.
15. Love MI, Huber W, Anders S. Moderated estimation of fold change and dispersion for RNA-seq data with DESeq2. *Genome Biol* **2014**;15:550.
16. Tsubaki M, Satou T, Itoh T, Imano M, Komai M, Nishinobo M, et al. Overexpression of MDR1 and survivin, and decreased Bim expression mediate multidrug-resistance in multiple myeloma cells. *Leuk Res* **2012**;36:1315–22.
17. Both J, Krijgsman O, Bras J, Schaap GR, Baas F, Ylstra B, et al. Focal chromosomal copy number aberrations identify CMTM8 and GPR177 as new candidate driver genes in osteosarcoma. *PLoS One* **2014**;9:e115835.
18. Gu P, Deng W, Lei M, Chang S. Single strand DNA binding proteins 1 and 2 protect newly replicated telomeres. *Cell Res* **2013**; 23(5):705-19.
19. Gordon N, Kleinerman ES. The Role of Fas/FasL in the Metastatic Potential of Osteosarcoma and Targeting this Pathway for the Treatment of Osteosarcoma Lung Metastases. *Cancer Treat Res* **2009**;152:497-508.
20. Choi YJ, Lee YS, Lee HW, Shim DM, Seo SW. Silencing of translation initiation factor eIF3b promotes apoptosis in osteosarcoma cells. *Bone Joint Res* **2017**;6:186–93.
21. Capobianco E, Mora A, La Sala D, Roberti A, Zaki N, Badidi E, et al. Separate and Combined Effects of DNMT and HDAC Inhibitors in Treating Human Multi-Drug Resistant Osteosarcoma HosDXR150 Cell Line. *PLoS One* **2014**;22;9(4):e95596.

22. Di Fiore R, Fanale D, Drago-Ferrante R, Chiaradonna F, Giuliano M, De Blasio A, et al. Genetic and molecular characterization of the human Osteosarcoma 3AB-OS cancer stem cell line: A possible model for studying osteosarcoma origin and stemness. *J Cell Physiol* **2013**;228:1189–201.
23. Li Y, Meng G, Guo Q. Changes in genomic imprinting and gene expression associated with transformation in a model of human osteosarcoma. *Exp Mol Pathol* **2008**;84:234–9.
24. Dos Santos Cavalcanti A, Meohas W, Ribeiro G de O, de Sá Lopes AC, Gholamin S, Razavi M, et al. Patient-derived osteosarcoma cells are resistant to methotrexate. *PLoS One* **2017**;12:e0184891.
25. Serra M, Reverter-Branchat G, Maurici D, Benini S, Shen J-N, Chano T, et al. Analysis of dihydrofolate reductase and reduced folate carrier gene status in relation to methotrexate resistance in osteosarcoma cells. *Ann Oncol* **2004**;15:151–60.
26. Hattinger CM, Stoico G, Michelacci F, Pasello M, Scionti I, Remondini D, et al. Mechanisms of gene amplification and evidence of coamplification in drug-resistant human osteosarcoma cell lines. *Genes Chromosomes Cancer* **2009**;48(4):289-309.
27. Selga E, Oleaga C, Ramírez S, de Almagro MC, Noé V, Ciudad CJ. Networking of differentially expressed genes in human cancer cells resistant to methotrexate. *Genome Med* **2009**;1(9):83.
28. Yang J, Guo W, Wang L, Yu L, Mei H, Fang S, et al. Cisplatin-resistant osteosarcoma cells possess cancer stem cell properties in a mouse model. *Oncol Lett* **2016**;12:2599–605.
29. Zahreddine H and Borden KL. Mechanisms and insights into drug resistance in cancer. *Front Pharmacol* **2013**;4:28.
30. Fanelli M, Hattinger CM, Vella S, Tavanti E, Michelacci F, Gudeman B, et al. Targeting ABCB1 and ABCC1 with their Specific Inhibitor CBT-1® can Overcome Drug Resistance in Osteosarcoma. *Curr Cancer Drug Targets* **2016**;16:261–74.
31. Xiang Q, Chen W, Ren M, Wang J, Zhang H, Deng DYB, et al. Cabozantinib suppresses tumor growth and metastasis in hepatocellular carcinoma by a dual blockade of VEGFR2 and MET. *Clin Cancer Res* **2014**;20:2959–70.
32. Piperno-Neumann S, Le Deley M-C, Rédini F, Pacquement H, Marec-Bérard P,

Petit P, et al. Zoledronate in combination with chemotherapy and surgery to treat osteosarcoma (OS2006): a randomised, multicentre, open-label, phase 3 trial. *Lancet Oncol* **2016**;17:1070–80.

33. Wang JJ, Li GJ. Relationship between RFC gene expression and intracellular drug concentration in methotrexate-resistant osteosarcoma cells. *Genet Mol Res* **2014**;13(3):5313-21.
34. Zhang Y, Mai Q, Zhang X, Xie C, Zhang Y. Microenvironment Signals and Mechanisms in the Regulation of Osteosarcoma. In: Honoki K, IntechOpen, editors. Osteosarcoma - Biology, Behavior and Mechanisms. London: InTech; **2017**. 430-462.
35. Creen V, Biteau K, Amiaud J, Dumars C, Guiho R, Vidal L, et al. Bone microenvironment has an influence on the histological response of osteosarcoma to chemotherapy: retrospective analysis and preclinical modeling. *Am J Cancer Res* **2017**;7(11):2333-2349.
36. Serra M, Scotlandi K, Manara MC, Maurici D, Lollini PL, De Giovanni C, et al. Establishment and characterization of multidrug-resistant human osteosarcoma cell lines. *Anticancer Res* **1993**;13:323–9.

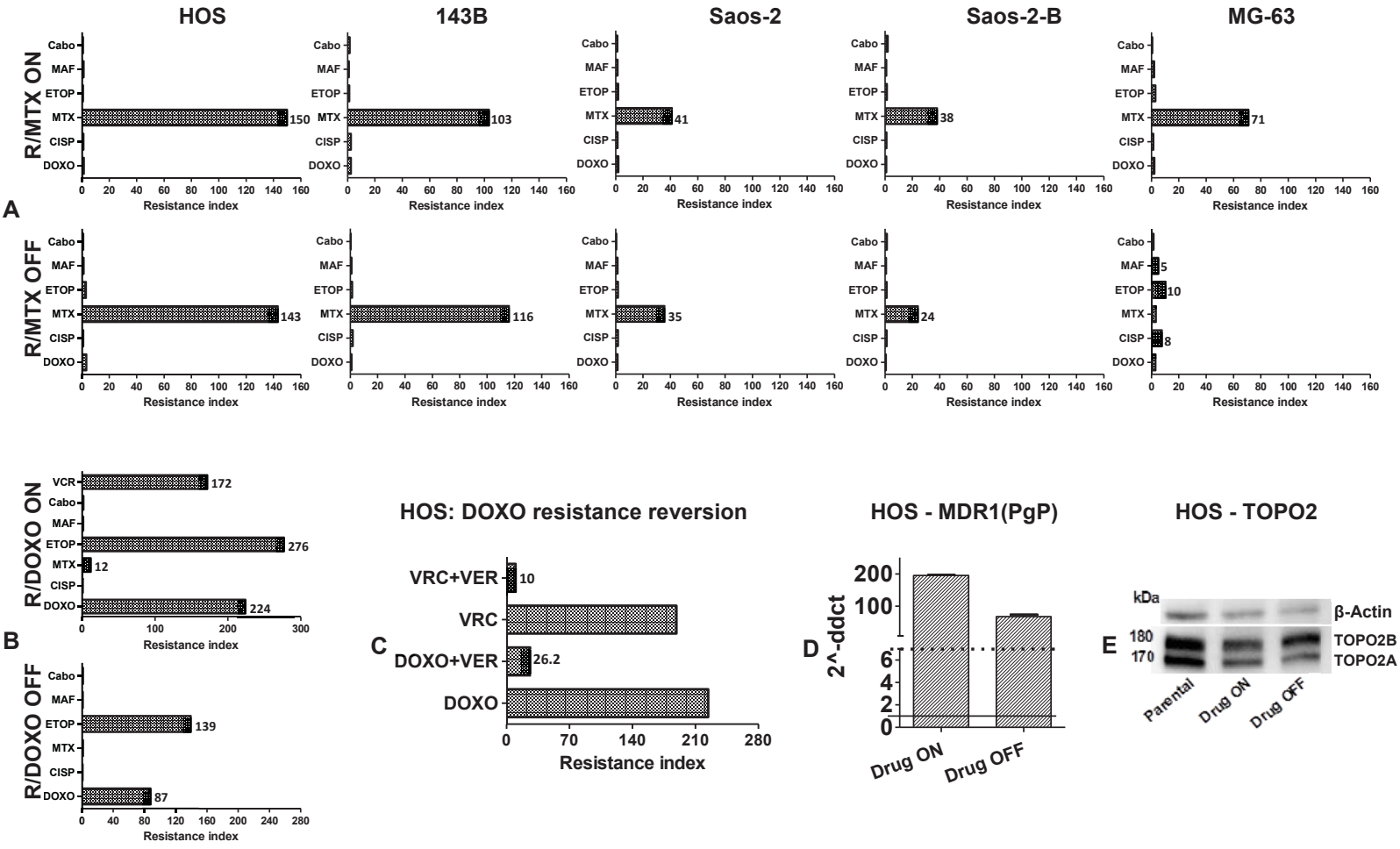
HOS
143B
Saos-2
Saos-2-B
MG-63
R/MTX ON
R/MTX OFF
A
Cabo
MAF
ETOP
MTX
CISP
DOXO
150
103
41
38
71
143
116
35
24
5
10
8
Resistance index
0 20 40 60 80 100 120 140 160

R/DOXO ON
R/DOXO OFF
B
VCR
Cabo
MAF
ETOP
MTX
CISP
DOXO
172
276
12
224
139
87
Resistance index
0 100 200 300
0 40 80 120 160 200 240 280

HOS: DOXO resistance reversion
C
VRC+VER
VRC
DOXO+VER
DOXO
10
26.2
Resistance index
0 70 140 210 280

HOS - MDR1(PgP)
D
2^-ddct
200
100
6
4
2
0
Drug ON
Drug OFF

HOS - TOPO2
E
kDa
180
170
β-Actin
TOPO2B
TOPO2A
Parental
Drug ON
Drug OFF

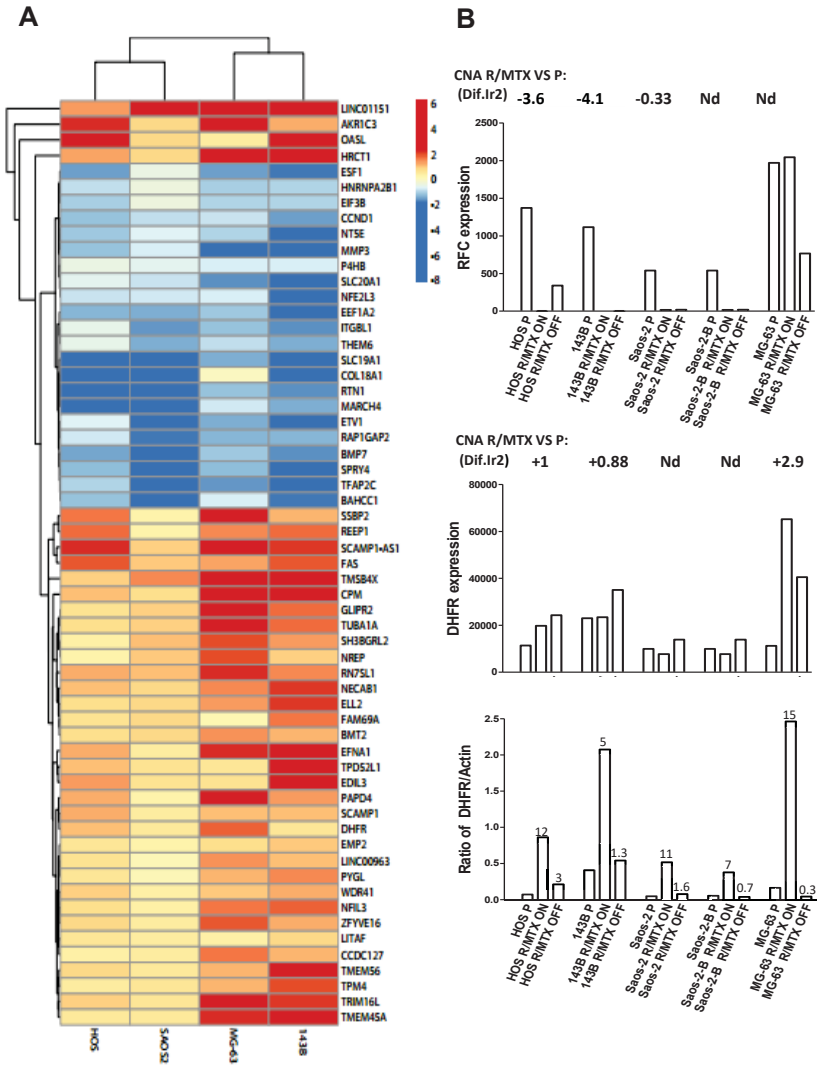
A
B
LINC01151
AKR1C3
OASL
HRCT1
ESF1
HNRNPA2B1
EIF3B
CCND1
NT5E
MMP3
P4HB
SLC20A1
NFE2L3
EEF1A2
ITGBL1
THEM6
SLC19A1
COL18A1
RTN1
MARCH4
ETV1
RAP1GAP2
BMP7
SPRY4
TFAP2C
BAHCC1
SSBP2
REEP1
SCAMP1-AS1
FAS
TMSB4X
CPM
GLIPR2
TUBA1A
SH3BGRL2
NREP
RN7SL1
NECAB1
ELL2
FAM69A
BMT2
EFNA1
TPD52L1
EDIL3
PAPD4
SCAMP1
DHFR
EMP2
LINC00963
PYGL
WDR41
NFIL3
ZFYVE16
LITAF
CCDC127
TMEM56
TPM4
TRIM16L
TMEM45A
HOS
SAOS2
MG-63
143B
6
4
2
0
-2
-4
-6
-8
CNA R/MTX VS P:
(Dif.Ir2)
-3.6
-4.1
-0.33
Nd
Nd
RFC expression
2500
2000
1500
1000
500
0
HOS P
HOS R/MTX ON
HOS R/MTX OFF
143B P
143B R/MTX ON
143B R/MTX OFF
Saos-2 P
Saos-2 R/MTX ON
Saos-2 R/MTX OFF
Saos-2-B P
Saos-2-B R/MTX ON
Saos-2-B R/MTX OFF
MG-63 P
MG-63 R/MTX ON
MG-63 R/MTX OFF
CNA R/MTX VS P:
(Dif.Ir2)
+1
+0.88
Nd
Nd
+2.9
DHFR expression
80000
60000
40000
20000
0
Ratio of DHFR/Actin
2.5
2.0
1.5
1.0
0.5
0.0
12
3
5
1.3
11
1.6
7
0.7
15
0.3

A

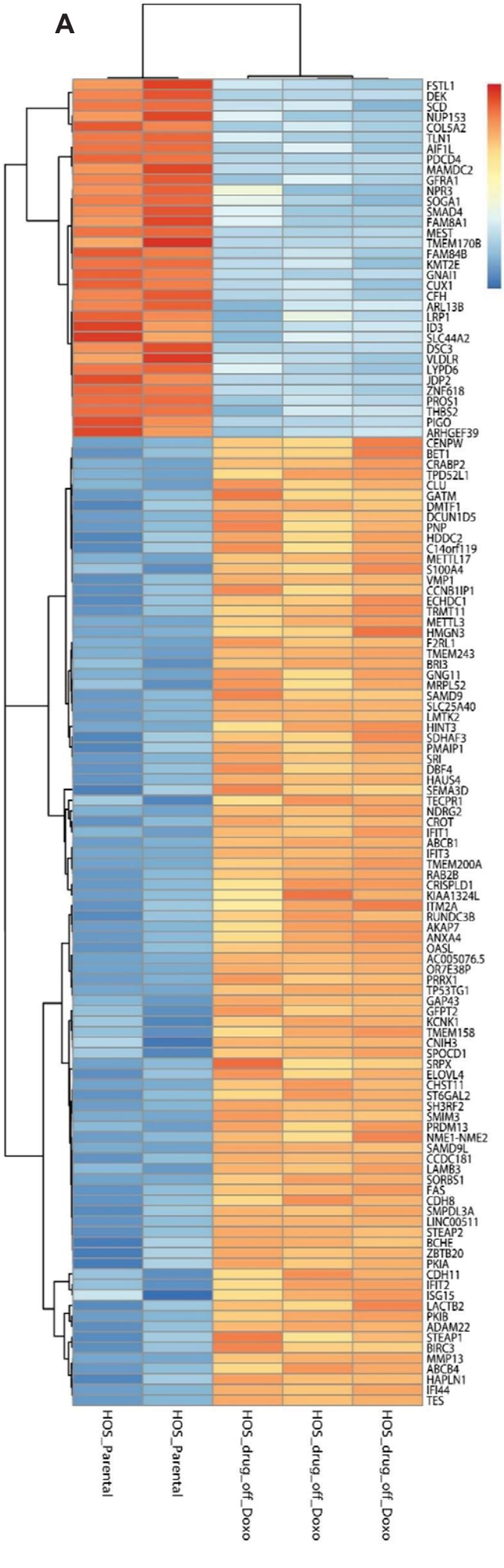

B

Entrez Gene Id	Gene Symbol	chr 7q21	chr 14q11	chr 11q22	Entrez	Source	Gene Description
10926	DBF4					S	DBF4 homolog (S. cerevisiae)
11257	TP53TG1					S	TP53 target 1 (non-protein coding)
154661	RUNDC3B					S	RUN domain containing 3B
222223	KIAA1324L					S	KIAA1324-like
223117	SEMA3D					S	sema domain, immunoglobulin domain (Ig), short basic domain, secreted, (semaphorin) 3D
26872	STEAP1					S	six transmembrane epithelial antigen of the prostate 1
389537	OR7E38P					S	olfactory receptor, family 7, subfamily E, member 38 pseudogene
5243	ABCB1					S	ATP-binding cassette, sub-family B (MDR/TAP), member 1
5244	ABCB4					S	ATP-binding cassette, sub-family B (MDR/TAP), member 4
53616	ADAM22					S	ADAM metallopeptidase domain 22
54677	CROT					S	carnitine O-octanoyltransferase
55972	SLC25A40					S	solute carrier family 25, member 40
6717	SRI					S	sorcin
79689	STEAP4					S	STEAP family member 4
390429	OR4N2					S	olfactory receptor, family 4, subfamily N, member 2
390431	OR4K2					S	olfactory receptor, family 4, subfamily K, member 2
4860	PNP					S	purine nucleoside phosphorylase
55017	C14orf119					S	chromosome 14 open reading frame 119
79544	OR4K1					S	olfactory receptor, family 4, subfamily K, member 1
85495	RPPH1					S	ribonuclease P RNA component H1
4319	MMP10					S	matrix metallopeptidase 10 (stromelysin 2)
4322	MMP13					S	matrix metallopeptidase 13 (collagenase 3)
84259	DCUN1D5					S	DCN1, defective in cullin neddylation 1, domain containing 5 (S. cerevisiae)

C

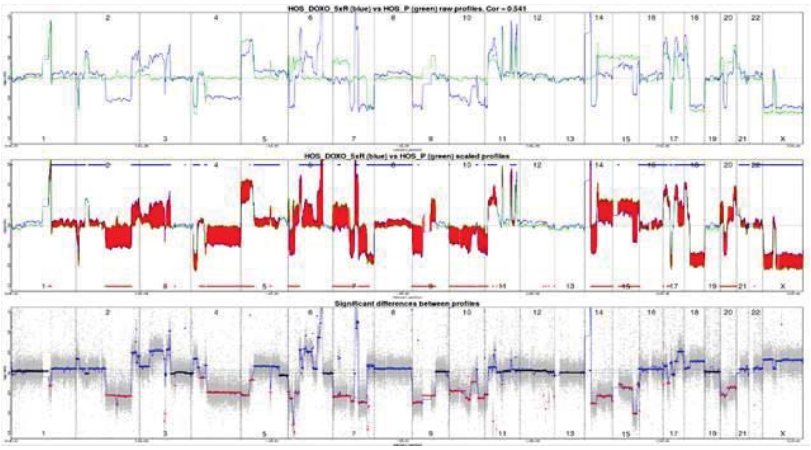

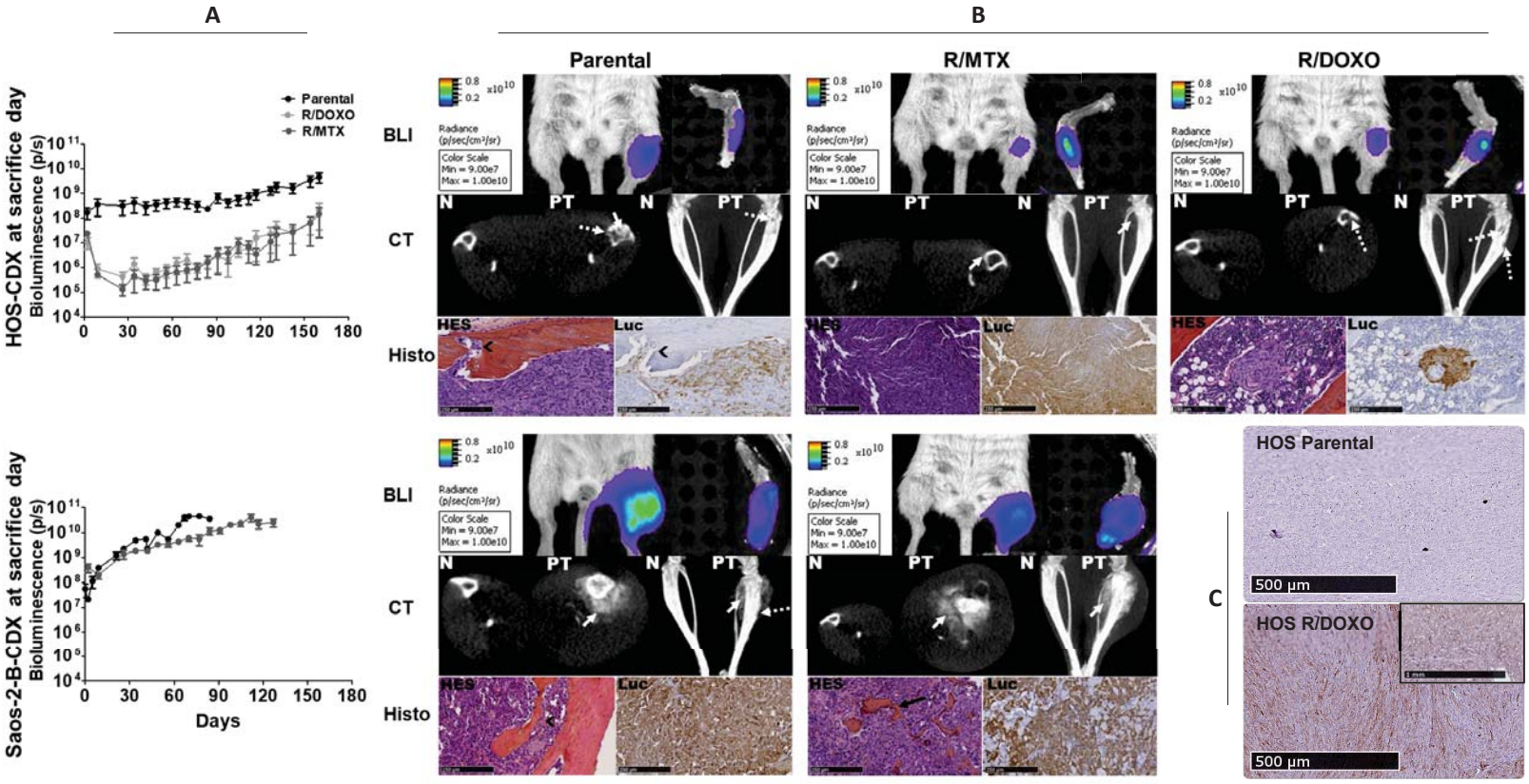
A
B
Parental
R/MTX
R/DOXO
HOS-CDX at sacrifice day
Bioluminescence (p/s)
Parental
R/DOXO
R/MTX
Saos-2-B-CDX at sacrifice day
Bioluminescence (p/s)
Days
BLI
CT
Histo
HES
Luc
N
PT
Radiance (p/sec/cm²/sr)
Color Scale
Min = 9.00e7
Max = 1.00e10
C
HOS Parental
HOS R/DOXO
500 µm

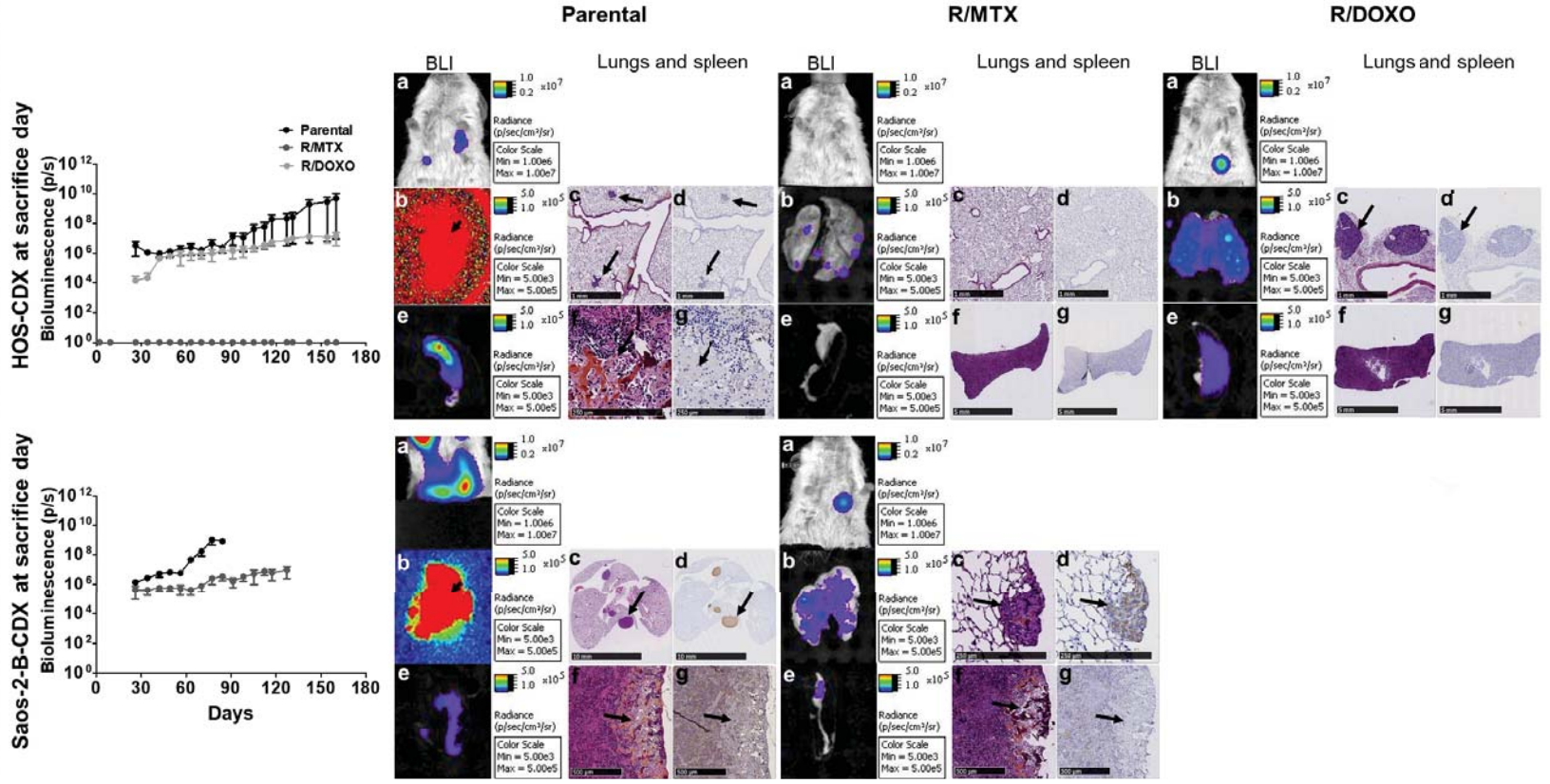
Parental
R/MTX
R/DOXO
BLI
Lungs and spleen
HOS-CDX at sacrifice day
Bioluminescence (p/s)
Days
Saos-2-B-CDX at sacrifice day
Radiance (p/sec/cm²/sr)
Color Scale
Min = 1.00e6
Max = 1.00e7
Min = 5.00e3
Max = 5.00e5

Cell lines Luc/mKate2	Parental		R/MTX		R/DOXO	
	Primary tumor	Metastases	Primary tumor	Metastases	Primary tumor	Metastases
HOS	5/5	5/5	8/8	4/8	4/6	4/6
Saos-2-B	5/6	5/6	4/4	4/4	-	-

	IC50			RI		IC50			RI	
	Parental	**R/MTX**		**R/MTX**		**Parental**	**R/DOXO**		**R/DOXO**	
Cell Lines	Before*	Before*	After*	Before*	After*	Before*	Before*	After*	Before*	After*
HOS	0.04	6.24	>100	156	>2000	0.06	11.3	2.09	212	41.8
Saos-2-B	0.05	1.93	2.05	37	34.2	NA	NA	NA	NA	NA